

Frequency width in predictions of windsea spectra and the role of the nonlinear solver



W. Erick Rogers^{a,*}, Gerbrant Ph. Van Vledder^{b,c}

^a Oceanography Division, Naval Research Laboratory, Stennis Space Center, MS, USA

^b Delft University of Technology, Civil Engineering and Geosciences, Environmental Fluid Mechanics, The Netherlands

^c BMT Argoss, Vollenhove, The Netherlands

ARTICLE INFO

Article history:

Available online 20 December 2012

Keywords:

Wind waves

Windsea

Spectral narrowness

Spectral width

Nonlinear interactions

Discrete interaction approximation

ABSTRACT

In this paper, the accuracy of predictions of the narrowness in frequency space of elevation spectra for wind-generated surface gravity waves is evaluated with the specific objective of determining the impact of the method for computing quadruplet interactions, S_{nl4} . Alternate metrics are presented for concise quantification of this narrowness and applied to a case study: a 10-day duration hindcast for Lake Michigan during 2002 conducted using the Discrete Interaction Approximation (DIA) for S_{nl4} . Under-prediction of frequency narrowness relative to observational data is clearly identifiable using non-concise methods. Two of four concise methods for quantifying spectral narrowness are found to adequately register this bias. By comparing with a hindcast that uses an expensive, exact solution for four-wave nonlinear interactions, it is determined that much of the bias can be attributed to the approximation used for the solution of these interactions in the first hindcast, which corresponds to the DIA, which is the solution method used today in nearly all routine, phase-averaged wave modeling.

Published by Elsevier Ltd.

1. Introduction

The so-called “third generation” (3G) model for wind-generated surface ocean gravity waves (Komen et al., 1984,1994; WAMDI Group, 1988; Tolman, 1991; Booij et al., 1999; WISE Group, 2007) is commonly used in engineering and operational forecasting applications (e.g. Jensen et al., 2002; Bidlot et al., 2002). In such applications, the most common and lowest order quantity predicted is waveheight, which is directly related to the total energy, m_0 , in a wave spectrum, $E(f, \theta)$, where E is the spectral density of sea surface elevation variance (energy), f is the wave frequency, and θ the wave direction: $m_0 = \iint E(f, \theta) df d\theta$. Increasingly, attention is being given to higher order features of the wave spectrum. This is motivated by steady progress in accuracy of predictions of simple waveheight, by the resulting desire to examine in greater detail the accuracy of $E(f, \theta)$ predicted by the models, and—perhaps most importantly—by the inherent utility of higher order quantities for specific applications. The present paper is specifically concerned with the accuracy of predictions of the width, in frequency space, of the non-directional spectrum $E(f) = \int E(f, \theta) d\theta$. Accurate predictions of the spectral narrowness are not only of scientific interest but also for engineering practice, where this property plays an important role in design formulas (Goda, 1985; Saulnier et al.,

2011). Particular effort is made to examine the impact of a particular approximation—the Discrete Interaction Approximation—on the accuracy of these predictions of frequency width. This approximation is made in the physics calculations of nearly all routine 3G wave model applications today, and is introduced below, subsequent to the introduction of the model physics in general.

The 3G wave models utilize a phase-averaged (spectral) description of wave conditions; the dependent variable being solved for in these models is most often the wave action density $N = E/\sigma$ (e.g. Bretherton and Garrett, 1968). Here, σ is the intrinsic angular frequency where “angular” refers to the relation $\sigma = 2\pi f$. Wave action N is solved in five dimensions, e.g. $N = N(f, \theta; \mathbf{x}, t)$, where \mathbf{x} denotes position and t time. The evolution of the wave spectrum is described by means of the radiative transfer equation (Gelci et al., 1956; Hasselmann, 1960), which can be written as:

$$\frac{\partial N}{\partial t} + \nabla \cdot cN = \frac{S_{tot}}{\sigma} = \frac{S_{in} + S_{ds} + S_{nl4} + S_{other}}{\sigma} \quad (1)$$

where c is the energy propagation velocity of the waves in each dimension ($c_x, c_y, c_\sigma, c_\theta$). The LHS of this equation accounts for kinematics, which are conservative, whereas on the RHS, S_{tot} represents dynamics. In deep water, it is generally accepted that wind-wave growth is primarily a result of three physical processes: atmospheric input from the wind to the waves, S_{in} , wave dissipation due to breaking S_{ds} , and nonlinear energy transfer between the wave components S_{nl4} . In finite depths, additional terms due to wave-bottom friction, depth-limited breaking and triad interactions

* Corresponding author. Address: Naval Research Laboratory, Code 7322, Bldg. 1009, Stennis Space Center, MS 39529, USA. Tel.: +1 228 688 4727; fax: +1 228 688 4759.

E-mail address: Erick.Rogers@nrlssc.navy.mil (W.E. Rogers).

become significant, and more terms can be formulated which may become important in particular circumstances, e.g. non-breaking dissipation or scattering from interaction with irregular bathymetry or with sea ice. Every 3G model includes the first three source terms, whereas the remaining source terms can vary from one model to another. All of these source terms are spectral functions. The reader is referred to WISE Group (2007) for a more complete overview of this technique of wave modeling.

Of these source terms, the present paper is primarily concerned with the term for four-wave nonlinear interactions, S_{nl4} (e.g. Hasselmann, 1962). In a developing sea, this term moves energy from frequencies just above the spectral peak to both lower and higher frequencies. The transfer to lower frequencies is a primary mechanism for frequency downshifting. The transfer to higher frequencies is balanced by wind input and white-capping dissipation resulting in power law-decay of wave action with frequency. This term has also been found to have a primary role in determining and stabilizing the spectral shape in general (Hasselmann et al. 1973; Young and Van Vledder, 1993). Unlike the other two primary source terms, the form of this term is known and can be solved for exactly (e.g. EXACT-NL, Hasselmann and Hasselmann, 1985) but is far too expensive for routine use, necessitating shortcuts, the most commonly used method being the Discrete Interaction Approximation (DIA) introduced in the seminal work by Hasselmann et al. (1985), which uses a relatively small subset of interactions but preserves the lowest order features of the exact approach. Since this period of rapid progress in the 1980s, much effort has been made in the wave model development community to alternately improve the accuracy of the DIA or improve the efficiency of the exact algorithms (WISE Group, 2007).

The qualitative impact of the DIA “shortcut” on model results has most often been presented for idealized scenarios (e.g. fetch-limited or turning winds), as this obviously facilitates comprehension of the most fundamental features. Hasselmann et al. (1985), for example, evaluate fetch-limited growth curves using the DIA and note that agreement of the more important scale parameters, total energy and peak frequency, were excellent, while two less important scale parameters were predicted less well; the one relating to spectral peakedness was reported as “somewhat smaller” than the ground truth. In subsequent years, considerable success has been achieved with 3G-models, especially in the context of those “more important scale parameters”, while at the same time the shortcomings of the DIA are receiving greater scrutiny (e.g. Van Vledder et al., 2000). These shortcomings are compensated by tuning of other source terms, thus hampering the development of 3G-models. In the simplest examples, the limitations of the DIA are illustrated by computing S_{nl4} using DIA for a fixed wave spectrum and comparing this with exact computations of S_{nl4} . This exercise reveals basic characteristics but is insufficient to anticipate practical outcomes in a time-stepping solution, because of the highly non-linear character of S_{nl4} . Instead, full model exercises are needed in which S_{nl4} is used in conjunction with other source terms. Some recent effort has been made to characterize the practical implications of the shortcut on realistic applications: Alves et al. (2002) examine fetch-limited spectra generated with implementations of DIA and exact- S_{nl4} in a 3G model, concluding that the use of the DIA algorithm constrains significantly the shape of 1-D frequency spectrum; Tolman (2011) presents applications in a synthetic hurricane and a storm event in Lake Michigan. One feature reported often is broader directional spreading with the DIA than with the full solution (Young et al., 1987; Van Vledder, 1990; Forristall and Ewans, 1998; Ardhuin et al., 2007; Tolman, 2011), broader frequency spectra (already visible in Hasselmann et al., 1985, their Figure 9) and an underestimation of the energy level at the spectral peak has also been reported (Tolman, 2011).

Tolman (2011) and others use the results from ‘exact’ calculations of S_{nl4} as ground truth. The soundness of this approach is obvious, since the accuracy of the ground truth cannot be questioned. However, these comparisons do not answer a particular, interesting question, which is, “can evidence of these known shortcomings of the DIA be noted, isolated, and proven in comparisons to observational data?”. This is the fundamental question of the present paper.

Rogers and Wang (2007), henceforth denoted “RW07” use a multi-month Lake Michigan hindcast with the SWAN model (Booij et al., 1999) to investigate possible bias in predictions of directional spreading relative to buoy observations. Their study was primarily motivated by previous claims that use of the DIA leads to overprediction of directional spreading. RW07 demonstrate overprediction of directional spreading above the peak in idealized simulations (using the ‘exact’ computations as ground truth) (their Figures 2 and 3), but did not find any overprediction of directional spreading in comparison to the buoy measurements (their Figures 8 and 9). A more positive but less emphasized feature of RW07 was the consistency of the results with regard to frequency width (the topic of the present paper). Specifically, in both the idealized comparisons against the ‘exact’ model (their Figure 2) and the buoy comparisons (their Figures 6 and 7), there is an overprediction of energy below the spectral peak, and so the spectrum is too broad.

RW07 could only indirectly attribute overprediction of frequency spreading to the DIA, since they did not apply the ‘exact’ S_{nl4} computations in their hindcast due to computational costs. This is, however, done by Ardhuin et al. (2007) in a hindcast for Duck, North Carolina. This was made possible (from a practical point of view) through the use of a finite element grid with relatively few grid points (CREST model, Ardhuin et al., 2001). These authors find that, in comparison to the ‘exact’ S_{nl4} -based model, the DIA-based model always has higher directional spreading (as expected), but this does not always lead to a larger error in comparison to buoy data. In cases where directional spreading predictions are made worse with ‘exact’ S_{nl4} , this is reasonably attributed to inaccuracies in the other source terms. Ardhuin et al. (2007) also mention in passing that the DIA would result in an overestimation of the growth of low-frequency waves if not for cancellation of errors via the other source terms, thus leading to overly broad frequency spectra.

Ardhuin et al. (2010) conducted Lake Michigan simulations similar to RW07, using the WAVEWATCH III® model (“WW3”, Tolman et al., 2002; Tolman, 2009). These simulations indicate overprediction of energy below the spectral peak similar to those shown in RW07 Figs. 6 and 7. Again, this was not positively attributed to the DIA. However, in the context of the Lake Michigan hindcasts, it suggests a robust feature, independent of modeling platform (SWAN, WW3) and $S_{in} + S_{ds}$ parameterizations (Komen et al., 1984; Bidlot et al., 2005; Ardhuin et al., 2010, or, as we will show, Rogers et al., 2012). The objective of the present study is to determine whether this overprediction of frequency width is positively attributable to the DIA.

Direct, side-by-side comparisons of one-dimensional wave spectra can be a useful method of presenting differences, or a means of careful model evaluation. However, in the context of routine or repetitive model validation exercises, it is often impractical. This is especially true in longer hindcasts with multiple locations of spectral observational data. In these cases, it is useful to utilize bulk parameters that effectively identify model error, and statistics can be calculated from these. For example, zero-moment wave height, H_{m0} is used to quantify total energy, and the spectral mean period (e.g. $T_{m,-1,0}$, $T_{m,0,1}$, $T_{m,0,2}$, see Appendix) is used to quantify a center (or centroid) of the frequency spectrum, variously defined to give more or less weight to frequencies further from that center. In this paper, existing methods for quantifying the narrowness in

frequency space of non-directional frequency spectra (as opposed to spectral width) are evaluated. We find that some methods are not sufficiently sensitive to problems with narrowness that are readily visible by eye.

This paper is organized as follows. The wave model is described in Section 2, and the utilized hindcast is described in Section 3. The methods of quantifying frequency narrowness are described in Section 4. In Section 5, overprediction of spectral width is demonstrated in a hindcast using DIA. In Section 6, an ‘exact’ S_{nl4} -based hindcast is analyzed and it is found that the bias in frequency width is reduced. Discussion and Conclusions are given in Sections 7 and 8.

2. Model description

The model platform is SWAN (Booij et al., 1999; SWAN, 2010) and the wind input (S_{in}), whitecapping (S_{ds}), and non-breaking dissipation (S_{swell}) parameterizations are taken from Rogers et al. (2012). We refer the reader to that paper for details, but the key features are briefly given here. The wind input term S_{in} is based on Donelan et al. (2006) and Tsagareli et al. (2010), developed from direct measurements of wind input at Lake George, Australia, with the wind drag coefficient C_d based on Hwang (2011). Dissipation from breaking (whitecapping), S_{ds} is based on Babanin et al. (2010) which is developed from Young and Babanin (2006), Tsagareli (2009), and Banner et al. (2000). S_{ds} is two-phase—insofar as it accounts for breaking of waves due to inherent instability and dissipation induced by the breaking of longer waves—and employs a breaking threshold, based on the Phillips (1958) saturation spectrum (the same concept was used earlier by others, such as Collins (1972) and Alves and Banner (2003)). In Rogers et al. (2012), the utilized form of S_{ds} is denoted as L4M4. Non-breaking dissipation, S_{swell} , is included to account for the slow attenuation of swell by non-breaking processes, and utilizes work by Ardhuin et al. (2009, 2010). In the notation of Rogers et al. (2012), $f_e = 0.006$ (controlling the strength of swell dissipation) is used in simulations described below. For four-wave nonlinear interactions S_{nl4} , we use methods available in SWAN (2010) without modification. The term is computed with either DIA or ‘exact’ computations. The latter is denoted “XNL” herein and is specifically the “Webb–Resio–Tracy” method (WRT) as implemented by van Vledder in SWAN, see Van Vledder (2002, 2006) and SWAN (2010).

3. Hindcast description: Lake Michigan 2002, 10-day simulation

Lake Michigan is a useful area for studying the impact of model physics, as it is mostly deep water (minimizing complications due to finite depth source terms), large enough to allow generation of dominant waves measurable using National Data Buoy Center (NDBC) buoys (e.g. $T_p = 6$ s), and enclosed, minimizing complications due to interaction with swell (older swells being non-existent). The latter feature is pertinent to the scope of this study, which is specific to windsea.

The Lake Michigan model simulations are set up as follows. The computational grid is approximately 252 km (east–west) by 496 km (north–south), with 4 km grid resolution. Directional resolution is 10° (36 bins), and a logarithmic frequency grid is used, with 35 frequencies from 0.07 to 1.97 Hz. The bathymetry, shown in Fig. 1, is provided at 2 km resolution by the NOAA Great Lakes Environmental Research Laboratory. Wind forcing is created from two NOAA NDBC buoys as described in Rogers et al. (2003) and RW07; the method assumes homogeneity in longitude and spatial variation in latitude determined by the buoys 45002 and 45007. JONSWAP (Hasselmann et al. 1973) bottom friction formula is used, though this is not expected to affect results, since this

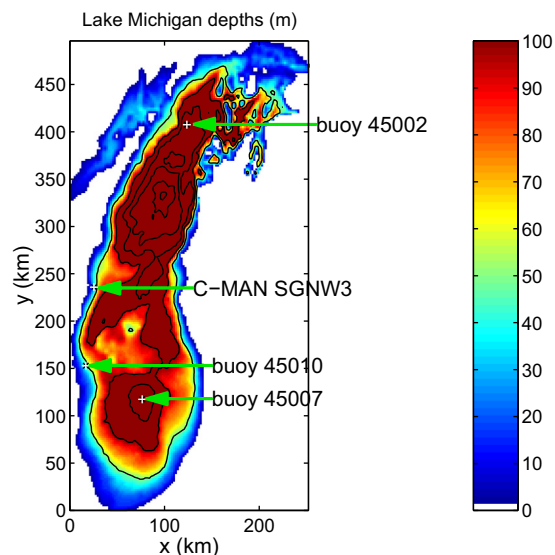


Fig. 1. Bathymetry of Lake Michigan (depths in meters). NOAA NDBC station locations are indicated. Buoy 45007 is used for model/data comparisons herein.

hindcast is predominately in deep water. The default numerics are used, a second order scheme with third order diffusion (see SWAN, 2010). Physics for S_{in} , S_{ds} , and S_{swell} are used as described in Section 2. The initial condition is from a ‘hotstart’ file created by the model using DIA for S_{nl4} , 0000 UTC 12 Oct. 2002 to 0000 UTC 13 Oct. 2002. The simulations used for comparisons are from 0000 UTC 13 Oct. 2002 to 0000 UTC 23 Oct. 2002 (10-day duration), using a time step of 6 min.

4. Methods

As mentioned in Section 1, the objective of the present study is to determine whether overprediction of frequency width is positively attributable to the DIA. A necessary step is to evaluate the utility of bulk parameters which can be used to quantify the narrowness in frequency space of the non-directional spectrum. In this section, four methods are described to quantify this property. All four methods are based on simple, direct calculation, mostly via integration, which is preferred over indirect methods, e.g. fitting to parametric spectra; this is a subjective decision and we do not dispute the merits of methods of the latter type.

Method A: Uses the method of SWAN (2010), as defined by Battjes and Van Vledder (1984). The calculation is:

$$Q_A \equiv \left| \int_{f_{min}}^{f_{max}} E(f) e^{i2\pi f \tau} df \right| / m_0 \quad (2)$$

where $m_0 = \int_{f_{min}}^{f_{max}} E(f) df$ and $\tau = T_{m,0.2}$ (defined in Appendix). The lower and upper bounds of the integration are denoted as f_{min} and f_{max} . As with other integral quantities, for any given comparison, f_{min} and f_{max} should be applied consistently: when comparing model and observations, this will often imply that the highest model frequencies are excluded from the calculation. In Battjes and Van Vledder (1984), Q_A is denoted as parameter κ and is referred to as a “shape parameter” for the purpose of predicting wave group statistics from a non-directional spectrum. The Battjes and Van Vledder (1984) paper is given as the source of the equation in SWAN (2010), although the actual source is Rice (1944). However, in SWAN (2010), the quantity is incorrectly referred to as “FSPR”, “the normalized frequency width of the spectrum (frequency spreading)”. Like the other methods described here, this parameter actually quantifies the narrowness of the spectrum and it ranges from 0 to 1.

Method B is:

$$Q_B \equiv (T_{m,0.2}/T_{m,-1,0})^2 \quad (3)$$

where $T_{m,0.2}$ and $T_{m,-1,0}$ are defined in the Appendix. Thus, it is the square of the ratio between $T_{m,0.2}$, which is often 70–90% of the peak period, and $T_{m,-1,0}$, which is usually much closer to the peak period. The closer this parameter is to one, the more peaked, or narrow, the frequency spectrum.

A similar quantity, $T_{m,0.1}/T_{m,-1,0}$ was used by Van Vledder et al. (2008), in studies of the Dutch Waddensea to assist in detection of areas where longer waves were dominant and where bi-modal spectra occurred. In the numerator of Q_B , $T_{m,0.2}$ is used here in preference to $T_{m,0.1}$ as it provides more separation from $T_{m,-1,0}$, and thus it is expected to have greater sensitivity to changes in shape.

Method C is:

$$Q_C \equiv \max(E_{fn})/T_{m,-1,0} \quad (4)$$

where:

$$E_{fn}(f) \equiv E(f)/m_0 \quad (5)$$

and:

$$\int_{f_{min}}^{f_{max}} E_{fn}(f) df = 1 \quad (6)$$

Thus Q_C is the peak of the function $E(f)$ after it has been normalized by the area under the same function.¹ The division by $T_{m,-1,0}$ is included to make the quantity dimensionless. This method was devised in this study following the formulation of the A parameter used by Babanin and Soloviev (1987, 1998a) to quantify narrowness of spectra in directional space. However, with the non-dimensionalization, we find that the formula is similar to those used by LeBlond et al. (1982), Belberov et al. (1983), Mansard and Funke (1990), and Babanin and Soloviev (1998b). Of the four methods used here, only this method includes a non-integral operation, the “ $\max(E_{fn})$ ” operation in (4). This implies that Q_C responds to spectral peakedness.

Method D is:

$$Q_D \equiv 2/m_0^2 \int_{f_{min}}^{f_{max}} f E^2(f) df \quad (7)$$

This is taken from Goda (1970, 1985). It has been referenced in the freak wave literature (Janssen, 2003) as “Goda’s peakedness factor Q_p ” with the Benjamin Feir Index being $BFI = k_0 Q_p \sqrt{m_0} 2\pi$. The higher Q_p , the more peaked the spectrum.

As it is less useful to evaluate higher order moments (in this case, spreading) in cases where the lower order moments are dissimilar, we only include points in the time series for which $e_H < 0.2$ and $e_T < 0.2$, where:

$$e_H = |H_{m0,obs} - H_{m0,model}|/H_{m0,obs} \quad (8)$$

$$e_T = |T_{m,-1,0,obs} - T_{m,-1,0,model}|/T_{m,-1,0,obs}$$

To familiarize with these quantities, we compare in Table 1 values calculated using the JONSWAP spectrum (see for example, Young, 1999, pg. 112) for different values of the JONSWAP spectral peakedness parameter γ , which many readers will be familiar with.² JONSWAP $\gamma = 1$ corresponds to fully developed seas, which tend to be relatively broad in frequency space, and JONSWAP $\gamma = 3.3$ corre-

¹ Apart from the division by the spectral wave period, one can recover the same value using the reciprocal value of the area of the function that is normalized by the peak value.

² Though it is not expected to have much impact on the calculations, for completeness, the other JONSWAP parameters used are: $f_p = 0.19$ and $\alpha = 0.02$, $\sigma_a = 0.07$, $\sigma_b = 0.09$ (see e.g., Young, 1999 for definition) with integration of frequencies from $f_{min} = 0.03$ Hz with grid spacing $\Delta f = 0.001$ Hz and an f^{-5} spectral tail.

Table 1

Example calculations of frequency narrowness parameters on JONSWAP spectra. In each case, two values for Q are given. The first value corresponds to upper bound of integration $f_{max} = 1.0$ Hz and the second value, in round brackets (), corresponds to $f_{max} = 0.4$ Hz.

JONSWAP γ	Narrowness			
	Q_A	Q_B	Q_C	Q_D
1.0	0.42 (0.37)	0.72 (0.83)	1.67 (1.72)	2.01 (2.25)
2.0	0.50 (0.47)	0.74 (0.85)	2.60 (2.66)	2.49 (2.74)
3.3	0.57 (0.55)	0.77 (0.87)	3.43 (3.49)	3.15 (3.41)
6.0	0.65 (0.65)	0.80 (0.89)	4.54 (4.60)	4.32 (4.59)
10.0	0.72 (0.72)	0.84 (0.91)	5.54 (5.59)	5.62 (5.87)
100.0	0.92 (0.92)	0.96 (0.98)	9.56 (9.58)	12.15 (12.25)

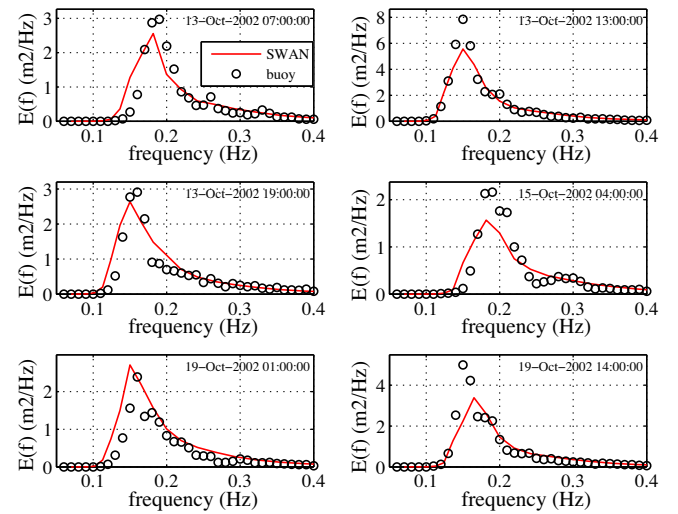


Fig. 2. Comparison of observed and computed non-directional spectra using the simulation with DIA for S_{n14} for six time periods.

sponds to younger seas, which tend to be relatively narrow in frequency space. Values of $\gamma > 6$ are not necessarily realistic for wind seas, but are included here for illustration.³ Also note that peak enhancement is a specific quantity associated with “overshoot” near the spectral peak (e.g. Young (1999), Figure 5.20), whereas spectral narrowness is a more general quantity that might be affected by other features of the spectrum, e.g. a bimodal frequency spectrum will tend to have a low spectral narrowness.

All four quantities are dimensionless. Separate calculations with the JONSWAP spectra (not shown) indicate that none of the Q parameters exhibit a significant dependence on the peak frequency f_p . With frequency distributions shaped like normal distributions, Q_C and Q_D exhibit strong and identical dependence on f_p (linear proportionality), a logical consequence of the form of the equations. Q_A and Q_B also exhibit some dependence on f_p using normal distributions. The differing behavior associated with use of normal distributions versus JONSWAP spectra is caused by the dependence of the JONSWAP spectrum on f_p beyond simply shifting the spectrum in frequency space.

The narrowness values in Table 1 are calculated with two alternate values for the upper limit of integration, $f_{max} = 1.0$ Hz and $f_{max} = 0.4$ Hz. This reveals some dependency of the parameters on f_{max} . Method B in particular is sensitive, which is not surprising given that it utilizes a higher order moment of the spectrum.⁴ Meth-

³ Using $\gamma > 6$ is actually a technique for providing SWAN with parameterized boundary forcing that is narrow, i.e. an unrealistically peaked wind sea can be used to approximate older swells, since the latter tend to be narrow in the real ocean.

⁴ The sensitivity would presumably be reduced by using $T_{m,0.1}$ instead of $T_{m,0.2}$.

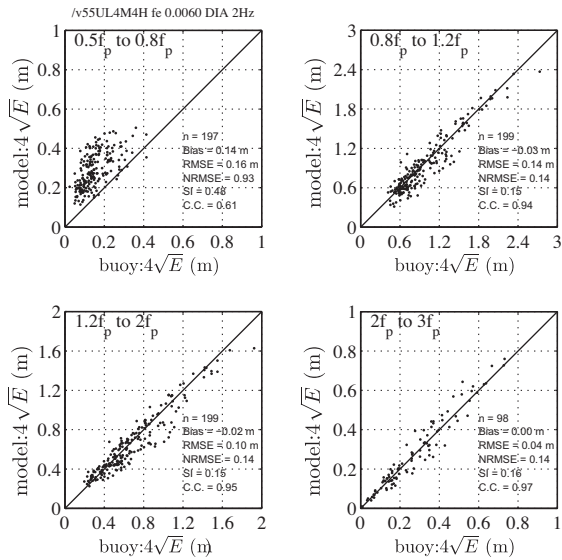


Fig. 3. Energy prediction estimates ($4\sqrt{m_0}$, in meters), divided into four relative frequency bands: DIA-based model vs. observations. Statistical quantities shown are in order: number of observations, bias, root-mean-square error, normalized root-mean-square error (calculation given in the Appendix), scatter index (standard deviation of errors divided by the mean of observations), and correlation coefficient CC calculated as shown in the Appendix.

od C appears to be the least sensitive. For example, the relative change from $f_{max} = 1.0$ Hz to $f_{max} = 0.4$ Hz with JONSWAP $\gamma = 1.0$ is -12% , $+15\%$, $+3\%$, and $+12\%$, for Q_A , Q_B , Q_C , and Q_D , respectively. At $\gamma = 6.0$, it is 0% , $+11\%$, $+1\%$, and $+6\%$.

5. Results using DIA

In this section, results from the model which employs the DIA for S_{nl4} are compared to observations from NOAA NDBC buoy 45007. Traditional bulk parameters such as waveheight and wave periods are only of peripheral concern in this study, but for sake of completeness, some are evaluated in the Appendix.

As a first step, the most direct method of comparison is used. Non-directional spectra $E(f)$ are compared for six time periods during the 10-day simulations in Fig. 2. These six times are selected as periods in which the absolute error of Q_C ,

$$E_{Q_C} = |Q_{C,model} - Q_{C,obs}| \quad (9)$$

matches the median E_{Q_C} for the 10-day simulation. Thus, this small subset of the larger simulation can be regarded as a typical representation of the whole, in the context of the narrowness quantity Q_C . Features of the DIA-based simulation are noticeably similar to those noted by RW07, Ardhuin et al. (2007) and Tolman (2011). Relative to the observations: (1) the energy level at the peak is low in five of the six plots, and (2) there is too much energy below the peak in at least three plots. However, as mentioned in Section 1, such qualitative comparisons cannot be directly used to generate statistics for long time series. Another form of comparison is to look at energy level, separated according to frequency relative to the peak, such as done in RW07 (their Figure 6). We can thereby verify that the DIA-based model exhibits the same overprediction of energy below the peak, as observed by that earlier study. This is shown in Fig. 3; the quantity compared is:

$$H_{m0,partial} = 4 \sqrt{\int_{f_1}^{f_2} E(f) df} \quad (10)$$

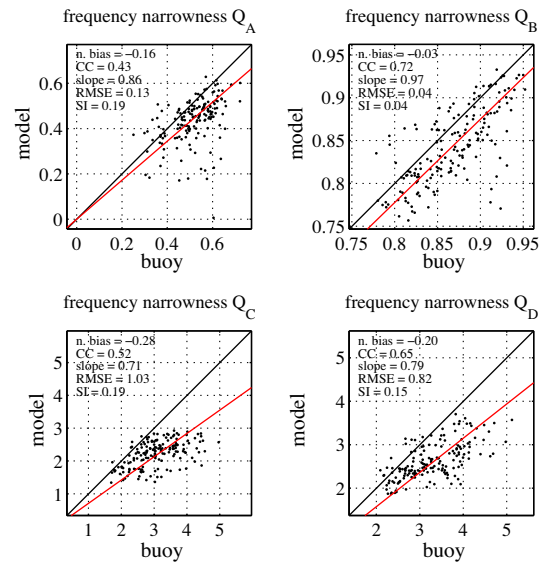


Fig. 4. Validation of frequency narrowness parameters Q_A , Q_B , Q_C , and Q_D . All model results shown are from the DIA simulation. The red line shows the linear best-fit relation. Statistical quantities shown are described in the Appendix. (For interpretation of the references to color in this figure legend, the reader is referred to the web version of this article.)

where frequencies f_1 and f_2 are indicated in each panel. The bias in the frequency range of $0.5 f_p < f < 0.8 f_p$ is $+14$ cm.⁵

The frequency narrowness parameters introduced in Section 4 are applied to evaluate the sensitivity of these four parameters to the problems visible in comparisons such as Fig. 2. This is done for the DIA-based simulation results in Fig. 4. In all cases, the upper bound on integration, f_{max} , is 0.4 Hz, corresponding to the buoy's upper limit. We find that parameters Q_A and Q_B do not show (or only weakly show) a bias that is apparent in the non-directional spectral comparisons. Parameters Q_C and Q_D do demonstrate this sensitivity. Q_C indicates the largest normalized bias, and it was demonstrated in Section 4 that this parameter has less sensitivity to the selection of f_{max} , so it is selected for all subsequent comparisons, though it is noted that Q_D is also suitable.

6. Results using XNL

The 10-day time simulation is repeated using XNL for S_{nl4} . For the other source terms, no changes are made, e.g. there is no re-calibration of the coefficients used in S_{ds} . Fig. 5 shows results from 6 h during the 10-day simulations, for comparison with Fig. 2. Qualitatively, the XNL-based simulation appears to provide a better match to the observations—especially in the context of the energy level at the peak, and amount of energy below the peak—in at least four of the six examples. A comparison of $H_{m0,partial}$, similar to Fig. 3, is made in Fig. 6. Whereas the bias in the frequency range of $0.5 f_p < f < 0.8 f_p$ is $+14$ cm using the DIA-based model, corresponding results with the XNL-based model indicate much smaller overall bias in energy below the peak, $+5$ cm. Thus, our data clearly support the interpretation that inaccuracies with the DIA contribute to the overprediction of energy below the peak.

To provide further support to this interpretation, the frequency narrowness parameters introduced in Section 4 are applied. Figs. 7 and 8 compare results using XNL versus those using DIA in terms of frequency narrowness parameters Q_C and Q_D . As shown in Fig. 7,

⁵ Using a similar simulation with the Komen et al., 1984 physics, we find a bias of $+11$ cm; using the 74-day simulation with Komen et al., 1984 physics, RW07 report a bias of $+9$ cm.

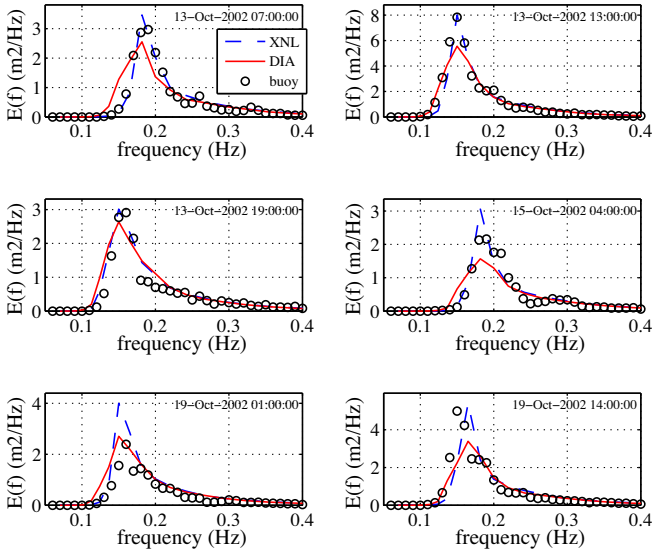


Fig. 5. Comparison of observed and computed non-directional spectra using the simulations with DIA and XNL for S_{nl4} for six time periods.

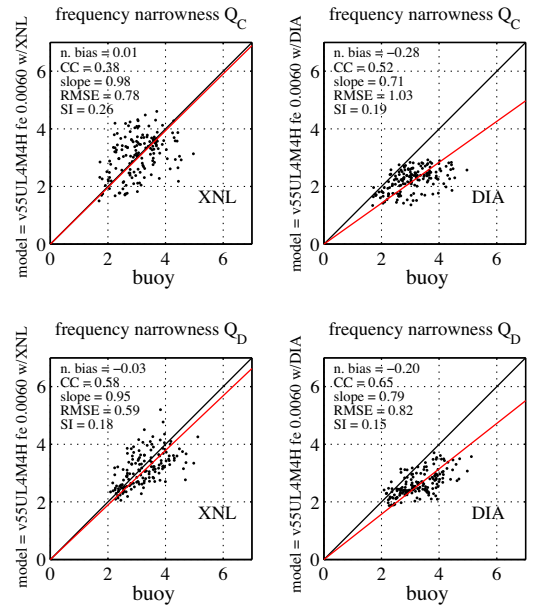


Fig. 7. Validation of frequency narrowness using the DIA and XNL for evaluating the quadruplet interactions. The frequency narrowness is quantified using parameter Q_C (upper panels) and Q_D (lower panels). Statistical quantities shown are described in the Appendix.

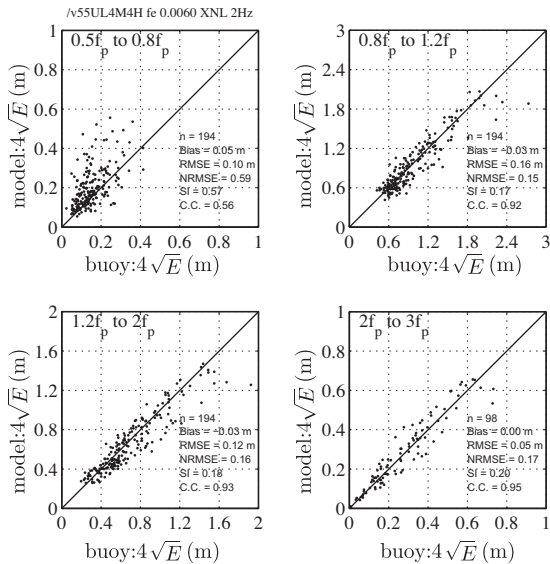


Fig. 6. Similar to Fig. 3, except for XNL-based model.

the bias in Q_C (upper panels of Fig. 7) is almost completely removed using XNL and the best-fit slope is near unity. However, random error, as quantified by the scatter index and correlation coefficient, actually increases; the cause of this is not known. Both the positive and negative consequences of replacing DIA with XNL are seen also in the Q_D comparison (lower panels of Fig. 7), but the consequences are not as pronounced as with Q_C . The time series comparison of Q_C , shown in Fig. 8, clearly illustrates the improved results by using XNL instead of the DIA.

7. Discussion

Model performance is often expressed in terms of bulk statistics of significant wave height H_{m0} and peak period T_p or a mean spectral period, e.g. $T_{m,0.2}$. For many applications these first order metrics are sufficient to judge model performance. However, with increasing requirements on model skill, other integral spectral parameters are gradually included in more model verification

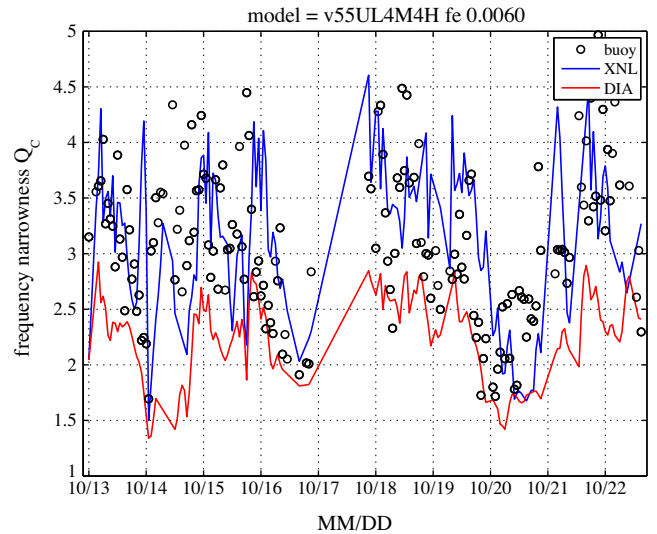


Fig. 8. As in upper panels of Fig. 7, except as time series comparison.

studies, such as the spectral period $T_{m,-1,0}$, the mean wave direction θ_m and the circular RMS directional spreading σ_θ . Together these parameters form a comprehensive set to assess model performance, but their error behavior can also be used to pinpoint model deficiencies.

In this study frequency narrowness is added to this list to investigate the effect of computational methods for nonlinear quadruplet interactions on the narrowness of the frequency spectrum. To that end various metrics quantifying spectral narrowness were investigated and one parameter was selected that is able to show a specific deficiency of the Discrete Interaction Approximation on the narrowness (or peakedness) of the frequency spectrum, and the over-prediction of spectral density below the peak frequency in particular. Based on simulations in Lake Michigan using the SWAN model and DIA and XNL parameterization of the quadruplet

Table 2
 Statistics for simulations of duration 10 days. The number of spectra used is indicated as n . Columns 2 and 4 correspond to the simulations discussed in the main text, and the physics described in Section 2 are denoted as RBW2012.

	XNL RBW2012		DIA RBW2012		DIA KHH $n_k = 2$	
	Full set	Subset	Full set	Subset	Full set	Subset
n	240	156	240	166	240	172
$H_{m,0}$ (m)						
Bias	-0.05	-0.01	-0.03	-0.00	0.00	0.03
RMSE	0.21	0.13	0.18	0.12	0.17	0.12
CC	0.93	0.97	0.95	0.98	0.96	0.98
$T_{m,0.1}$ (s)						
Bias	-0.18	-0.15	-0.10	-0.06	0.08	0.15
RMSE	0.37	0.28	0.33	0.23	0.32	0.26
CC	0.85	0.92	0.86	0.94	0.89	0.95
$T_{m,0.2}$ (s)						
Bias	-0.18	-0.15	-0.11	-0.07	0.06	0.12
RMSE	0.35	0.27	0.31	0.21	0.29	0.23
CC	0.85	0.91	0.86	0.94	0.89	0.95
$T_{m,-1.0}$ (s)						
Bias	-0.18	-0.14	-0.07	-0.01	0.12	0.20
RMSE	0.41	0.31	0.37	0.26	0.38	0.33
CC	0.85	0.92	0.86	0.93	0.88	0.94
Q_A						
Norm. bias	-0.04	-0.06	-0.14	-0.16	-0.09	-0.11
CC	0.43	0.51	0.42	0.43	0.46	0.44
Slope	0.94	0.94	0.86	0.86	0.91	0.90
Q_B						
Norm. bias	-0.00	-0.01	-0.02	-0.03	-0.02	-0.03
CC	0.74	0.79	0.69	0.72	0.69	0.72
Slope	1.00	0.99	0.98	0.97	0.98	0.97
Q_C						
Norm. bias	-0.01	0.01	-0.27	-0.28	-0.26	-0.26
CC	0.34	0.38	0.47	0.52	0.49	0.49
Slope	0.96	0.98	0.71	0.71	0.73	0.73
Q_D						
Norm. bias	-0.01	-0.03	-0.17	-0.20	-0.16	-0.18
CC	0.53	0.59	0.56	0.66	0.59	0.65
Slope	0.95	0.95	0.80	0.79	0.82	0.81

interactions, we are able to show the applicability of the spectral narrowness parameter Q_C to illustrate a potential weak point of the DIA.

Other metrics for frequency width, not shown here, have been used with success. For example, in cases of uni-modal spectra, the distance (in Hz) between f_1 and f_2 can be used, where $E(f_1) = E(f_2) = 0.5 \max(E(f))$. Or, the spectrum can be normalized and treated as a pseudo-probability distribution function, and standard deviation-like parameter can then be calculated. Such parameters might in fact be preferred to the Q parameters since the units (Hz) are more tangible. Saulnier et al. (2011) recently provided an excellent overview of a number of metrics, both dimensional and non-dimensional. As mentioned already, fitting a γ parameter to the JONSWAP has been used successfully in the past, e.g. by Hasselmann et al. (1985). Experiments with 16 alternate metrics have been performed and will be documented separately in a report focused on metrics.

Validation of higher order moments of directional and non-directional spectra introduces new challenges. Not only are the models normally less reliable for prediction of these moments, but such applications also require more fidelity from our observational datasets, perhaps pushing to their limits in some cases. Van Vledder and Battjes (1992) raise concerns about the statistical properties of narrowness metric Q_D , which is based on Goda (1970, 1985). In short, though the metric can be quite useful for application to model spectra, application to measured spectra is less reliable due to sensitivity to the amount of smoothing used in creating the spectra. We anticipate that this criticism would also

apply to method C as it may affect the peak value $\max(E_{\theta})$. As such, validation with these metrics (such as our Fig. 7) must be interpreted in the context of the dataset used. Further, disparate observational datasets should not be combined when creating statistics for validation: the statistics should be treated separately. This is in contrast to treatment of traditional quantities such as wave height.

Though much more useful than subjective visual comparison of non-directional spectra, comparisons such as Fig. 3 still have limitations. The most significant limitation is the requirement to identify the spectral peak, and that all energy is evaluated according to its position relative to this single peak. This is easily justified in environments such as Lake Michigan, which is typically dominated by windsea.⁶ However, in the open ocean, it is much more common to have multiple peaks due to swell, and so these comparisons are impossible without first separating the windsea from swell. The four narrowness parameters applied here, by contrast, still have meaning in the case of bimodal spectra, just as waveheight H_{m0} has meaning. Even so, it is felt that application of a windsea/swell separation algorithm (e.g. Gerling, 1992; Hanson and Phillips, 2001) prior to calculations of narrowness will often be worthwhile, and it obviously necessary if windsea (e.g. impact of source terms on windsea) is being studied.

In Section 5, the overprediction of wave energy below the spectral peak using a DIA-based model is documented, using the phys-

⁶ This dominance is not absolute, however: in the Great Lakes, because of their size, buoy measurements sometimes indicate two peaks during rapidly rotating winds, implying a new windsea and old windsea (alternately named young swell) component.

Table 3

Statistics for simulations of duration 74 days using DIA. The third column (KHH $n_k = 2$, full set) is essentially the same simulation as used by RW07.

	RBW2012		KHH $n_k = 2$		KHH $n_k = 1$	
	Full set	Subset	Full set	Subset	Full set	Subset
n	1685	1092	1688	1089	1688	912
$H_{m,0}$ (m)						
Bias	-0.02	-0.01	0.02	0.01	-0.12	-0.06
RMSE	0.17	0.12	0.17	0.12	0.21	0.14
CC	0.96	0.97	0.96	0.98	0.95	0.98
$T_{m,0.1}$ (s)						
Bias	-0.07	-0.07	0.11	0.12	-0.36	-0.26
RMSE	0.33	0.24	0.34	0.26	0.51	0.35
CC	0.90	0.94	0.90	0.94	0.88	0.95
$T_{m,0.2}$ (s)						
Bias	-0.08	-0.08	0.09	0.10	-0.35	-0.26
RMSE	0.31	0.22	0.32	0.24	0.49	0.34
CC	0.90	0.94	0.90	0.94	0.88	0.95
$T_{m,-1.0}$ (s)						
Bias	-0.05	-0.03	0.15	0.16	-0.37	-0.23
RMSE	0.36	0.26	0.40	0.32	0.55	0.35
CC	0.90	0.94	0.91	0.94	0.87	0.95
Q_A						
Norm. bias	-0.11	-0.13	-0.08	-0.08	-0.08	-0.14
CC	0.76	0.70	0.76	0.68	0.63	0.61
Slope	0.88	0.87	0.90	0.92	0.88	0.83
Q_B						
Norm. bias	-0.02	-0.02	-0.02	-0.02	-0.00	-0.02
CC	0.84	0.85	0.83	0.84	0.74	0.80
Slope	0.98	0.98	0.98	0.98	0.99	0.98
Q_C						
Norm. bias	-0.29	-0.28	-0.32	-0.25	-0.30	-0.30
CC	0.53	0.61	0.57	0.63	0.58	0.55
Slope	0.70	0.70	0.71	0.73	0.69	0.68
Q_D						
Norm. bias	-0.28	-0.20	-0.34	-0.17	-0.27	-0.19
CC	0.46	0.78	0.52	0.81	0.53	0.74
Slope	0.80	0.80	0.80	0.81	0.83	0.78

ics of Rogers et al. (2012) for S_{in} and S_{ds} . The same behavior is documented for longer duration simulations and more traditional forms of S_{in} and S_{ds} in the Appendix. Further, the behavior is observed by Ardhuin et al. (2010) using a third set of physics, and a different model, WAVEWATCH III, applied in Lake Michigan. Ardhuin et al. (2007) observe similar behavior using a third model, applied at the North Carolina continental shelf. Therefore, it may be a robust feature, not specific to a particular model, or physics package, or hindcast. Herein, this behavior is partially attributed to the DIA by applying the same hindcast with XNL. In this study, only one model (SWAN), one hindcast (Lake Michigan), and one set of physics are employed. It is not demonstrated that utilization of XNL in another model, hindcast, or with other physics would yield the same improvement to model agreement with observations. However, it is noted that narrower or more peaked spectra with XNL is a robust characteristic of comparisons between DIA and XNL (e.g. Hasselmann et al., 1985, RW07, Tolman, 2011), so it is reasonable to expect that where this robust bias feature exists, application of XNL may improve agreement with observations.

8. Conclusions

We summarize the results of this study as follows:

- From analysis of hindcasts for Lake Michigan presented in this study, as well as prior cited works, overprediction of energy below the spectral peak—resulting in overly broad non-directional spectra—may be a consistent feature of 3G models which utilize the Discrete Interaction Approximation (DIA) for S_{nl4} .

- Using a 10-day hindcast for Lake Michigan here, and in prior idealized computations (Hasselmann et al., 1985, RW07), we find a consistent outcome: the models which use exact computations for S_{nl4} produce more narrow frequency spectra than comparable simulations that use the DIA for S_{nl4} .
- Four methods are presented for quantifying the narrowness of a spectrum in frequency space. Those denoted as Methods C and D presented here are found to be most useful, insofar as they are found to be suitably sensitive to the narrowness that is clear from visual inspection. Method C is a frequency analog of a method proposed by Babanin and Soloviev (1987, 1998a) for quantifying directional width. Method D employs the peakedness factor used by Goda (1970, 1985).
- The narrowness quantity associated with Method C agrees well—in the mean—with observed frequency spectra if exact computations are used for S_{nl4} in the 10-day hindcast presented.
- Scatter of the same narrowness quantity for the same simulation is, however, worse when exact computations are used for S_{nl4} .

Acknowledgments

The authors thank Dr. David Wang and anonymous reviewers for constructive comments and suggestions. Dr. Wang was especially helpful in pointing out earlier work with metrics. Results from this study were first shared with the wave modeling community by Prof. Alex Babanin at the 2011 Waves in Shallow Environments meeting, for which the authors are grateful. This work was

supported by the Office of Naval Research under the National Ocean Partnership Program.

Appendix A. Additional error statistics, including results with alternate physics

Though not a specific goal of this study, it is useful to document the performance of the models in terms of conventional quantities, wave height and mean period. As mentioned earlier, validation of higher order moments is more meaningful in cases where lower order moments are in good agreement. In this appendix, we include the following set of quantities:

1. Significant waveheight, $H_{m0} = 4\sqrt{m_0} = 4\sqrt{\int E(f)df}$.
2. Mean spectral period, $T_{m,0.1} = \int E(f)df / \int fE(f)df$.
3. mean spectral period, $T_{m,0.2} = \sqrt{\int E(f)df / \int f^2 E(f)df}$.
4. Mean spectral period, $T_{m,-1.0} = \int f^{-1} E(f)df / \int E(f)df$.
5. Spectral narrowness (or peakedness) parameters, Q_A , Q_B , Q_C , and Q_D as defined in Section 4.

In all integrals, the lower and upper bounds on integration f_{min} and f_{max} are implied.

Statistics used to quantify error are the following:

1. Bias, i.e. the mean error.
2. Normalized bias, the bias divided by the mean of the observations.
3. Root-mean-square error (RMSE).
4. Slope of a least-squares fit that passes through the origin.
5. Pearson's correlation coefficient (CC) as computed by, for example, Cardone et al. (1996), Ardhuin et al. (2010), $CC = \frac{\langle(O-O)(M-M)\rangle}{\sqrt{\langle(O-O)^2}\sqrt{\langle(M-M)^2}\rangle}$, where $\bar{}$ and $\langle \rangle$ indicate a mean, O are observations and M are model values.
6. Normalized root-mean-square error, as given by Ardhuin et al. (2010), $NRMSE = \sqrt{\frac{\sum(O-M)^2}{\sum O^2}}$
7. Scatter index SI, the standard deviation of errors divided by the mean of observations.

It is also useful to present results using an alternate physics package, especially since the physics used in this paper are relatively new. This is done here using the Komen et al. (1984) physics (denoted here as KHH) with the minor adjustment suggested by Rogers et al. (2003). [The dependence on relative wavenumber $n_k = 2$ is used, where $n_k = 1$ is favored by Komen et al. (1984). Here, $S_{ds}(f) \propto (k/k_m)^{n_k}$, and k_m is the mean wavenumber]. The physics have deficiencies, especially with regard to non-physical interaction between windsea and swell, and non-physical spectral slope in the high-frequency tail, but as shown by Rogers et al. (2003) and RW07, using $n_k = 2$ can be highly skillful in the Lake Michigan simulations. For these physics, calculations were performed only with the DIA.

For sake of completeness, we present statistics with and without the sub-selection of spectra according to e_H and e_T as described in Section 4.

Statistics for the three types of model runs are given in Table 2. The results for the DIA and XNL based runs support the conclusions about the applicability of the various narrowness parameters presented in Section 4. The results for the DIA based runs, using the 'old' and 'new' physics package are close to each other; this suggests that the applicability of the narrowness parameters does not depend on the type of physics package. The results also show that the DIA-based model runs have better performance (in terms

of integral wave height and period measures) than the XNL based runs. This is probably due to the fact that the XNL based model was not calibrated, but we deem this not essential for our purpose. We also present statistics for a longer simulation, that used by RW07. These are given in Table 3. For this 74-day simulation, calculations were performed only with the DIA. As already concluded for the results presented in Table 2, the type of input/dissipation physics package has practically no effect on the applicability of the narrowness parameters.

References

- Alves, J.H.G.M., Banner, M.L., 2003. Performance of a saturation-based dissipation-rate source term in modeling the fetch-limited evolution of wind waves. *J. Phys. Oceanogr.* 33, 1274–1298.
- Alves, J.H.G.M., Greenslade, D.J.M., Banner, M.L., 2002. Impact of a Saturation-dependent dissipation source function on operational hindcasts of wind-waves in the Australian region. *J. Atmos. Oceanic Technol.* 8 (4), 239–267.
- Ardhuin, F., Herbers, T.H.C., O'Reilly, W.C., 2001. A hybrid Eulerian–Lagrangian model for spectral wave evolution with application to bottom friction on the continental shelf. *J. Phys. Oceanogr.* 31 (6), 1498–1516.
- Ardhuin, F., Herbers, T.H.C., Van Vledder, G.Ph., Watts, K.P., Jensen, R.E., Graber, H.C., 2007. Swell and slanting fetch effects on wind wave growth. *J. Phys. Oceanogr.* 37, 908–931.
- Ardhuin, F., Chapron, B., Collard, F., 2009. Observation of swell dissipation across oceans. *Geophys. Res. Lett.* 36, L06607. <http://dx.doi.org/10.1029/2008GL037030>.
- Ardhuin, F., Rogers, E., Babanin, A., Filipot, J.-F., Magne, R., Roland, A., van der Westhuysen, A., Queffelec, P., Lefevre, J.-M., Aouf, L., Collard, F., 2010. Semi-empirical dissipation source functions for ocean waves: Part I, definitions, calibration and validations. *J. Phys. Oceanogr.* 40, 1917–1941.
- Babanin, A.V., Soloviev, Yu.P., 1987. Parameterization of width of directional energy distributions of wind-generated waves at limited fetches. *Izv. Atmos. Oceanic Phys.* 23 (8), 645–651.
- Babanin, A.V., Soloviev, Yu.P., 1998a. Variability of directional spectra of wind-generated waves, studied by means of wave staff arrays. *Marine Freshwater Res.* 49 (2), 89–101.
- Babanin, A.V., Soloviev, Yu.P., 1998b. Field investigation of transformation of the wind wave frequency spectrum with fetch and the stage of development. *J. Phys. Oceanogr.* 28, 563–576.
- Babanin, A.V., Tsagareli, K.N., Young, I.R., Walker, D.J., 2010. Numerical investigation of spectral evolution of wind waves. Part 2. Dissipation function and evolution tests. *J. Phys. Oceanogr.* 40, 667–683.
- Banner, M.L., Babanin, A.V., Young, I.R., 2000. Breaking probability for dominant waves on the sea surface. *J. Phys. Oceanogr.* 30, 3145–3160.
- Battjes, J.A., Van Vledder, G.Ph., 1984. Verification of Kimura's theory for wave group statistics. In: *Proceedings of the 19th International Conference on Coastal Engineering*, ASCE, Houston, Texas, pp. 642–648.
- Belberov, Z.K., Zhurbas, V.M., Zaslavskii, M.M., Lobisheva, L.G., 1983. Integral characteristics of wind wave frequency spectra. Interaction of Atmosphere, Hydrosphere, and Lithosphere in Near-Shore Zone of the Sea (in Russian, English summary). In: Belberov, Z., Zahariev, V., Kuznetsov, O., Pykhov, N., Filyushkin, B., Zaslavskii, M. (Eds.), *Bulgarian Academy of Science Press*, pp. 143–154.
- Bidlot, J.-R., Holmes, D.J., Wittmann, P.A., Lalbeharry, R., Chen, H.S., 2002. Intercomparison of the performance of operational ocean wave forecasting systems with buoy data. *Weather Forecasting* 17 (2), 287–310.
- Bidlot, J., Janssen, P.A.E.M., Abdalla, S., 2005. A revised formulation for ocean wave dissipation in CY25R1. Technical Report Memorandum R60.9/JB/0516, Research Department, ECMWF, Reading, U.K., pp. 35.
- Booij, N., Ris, R.C., Holthuijsen, L.H., 1999. A third-generation wave model for coastal regions, Part 1: model description and validation. *J. Geophys. Res.* 104 (C4), 7649–7666.
- Bretherton, F.P., Garrett, C.J.R., 1968. Wavetrains in inhomogeneous moving media. *Proc. Royal Soc. London A* 302, 529–554.
- Cardone, V.J., Jensen, R.E., Resio, D.T., Swail, V.R., Cox, A.T., 1996. Evaluation of contemporary ocean wave models in rare extreme events: the "Halloween Storm" of October 1991 and the "Storm of the Century" of March 1993. *J. Atmos. Oceanic Technol.* 13, 198–230.
- Collins, J.I., 1972. Prediction of shallow water spectra. *J. Geophys. Res.* 77 (15), 2693–2707.
- Donelan, M.A., Babanin, A.V., Young, I.R., Banner, M.L., 2006. Wave follower field measurements of the wind input spectral function. Part II. Parameterization of the wind input. *J. Phys. Oceanogr.* 36, 1672–1688.
- Forristall, G.Z., Ewans, K.C., 1998. Worldwide measurements of directional wave spreading. *J. Atmos. Oceanic Technol.* 15, 440–469.
- Gelci, R., Cazale, H., Vassal, J., 1956. Utilisation des diagrammes de propagation a la prevision energetique de la houle, Bulletin d'information du Comite d'Océanographie et d'Etude des Cotes, pp. 169–197.
- Gerling, T.W., 1992. Partitioning sequences and arrays of directional wave spectra into component wave systems. *J. Atmos. Oceanic Technol.* 9, 444–458.
- Goda, Y., 1970. 1. Numerical experiments on wave statistics with spectral simulation. Report of the Port and Harbour Research Institute. vol. 9(3), pp. 57.

- Goda, Y., 1985. Random Sea and Design of Maritime Structures. Univ. Tokyo Press, pp. 323.
- Hanson, J.L., Phillips, O.M., 2001. Automated analysis of ocean surface directional wave spectra. *J. Atmos. Oceanic Technol.* 18, 277–293.
- Hasselmann, K., 1960. Grundgleichungen der Seegangsvoraussage. *Schiffstechnik* 7 (39), 191–195.
- Hasselmann, K., 1962. On the nonlinear energy transfer in a gravity-wave spectrum. Part 1. General theory. *J. Fluid Mech.* 12, 481–500.
- Hasselmann, S., Hasselmann, K., 1985. Computations and parameterizations of the nonlinear energy transfer in a gravity-wave spectrum. Part I. A new method for efficient computations of the exact nonlinear transfer integral. *J. Phys. Oceanogr.* 15, 1369–1377.
- Hasselmann, S., Hasselmann, K., Allender, J.H., Barnett, T.P., 1985. Computations and parameterizations of the nonlinear energy transfer in a gravity-wave spectrum. Part II: Parameterizations of the nonlinear energy transfer for application in wave models. *J. Phys. Oceanogr.* 15, 1378–1391.
- Hasselmann, K., Barnett, T.P., Bouws, E., Carlson, H., Cartwright, D.E., Enke, K., Ewing, J.A., Gienapp, H., Hasselmann, D.E., Kruseman, P., Meerburg, A., Muller, P., Olbers, D.J., Richter, K., Sell, W., Walden, H., 1973. Measurements of wind-wave growth and swell decay during the Joint North Sea Wave Project (JONSWAP). *Dtsch. Hydrogr. Z. Suppl.* 12, 1–95.
- Hwang, P.A., 2011. A note on the ocean surface roughness spectrum. *J. Atmos. Oceanic Technol.* 28, 436–443.
- Janssen, P.A.E.M., 2003. Nonlinear four-wave interactions and freak waves. *J. Phys. Oceanogr.* 33, 863–884.
- Jensen, R.E., Wittmann, P.A., Dykes, J.D., 2002. Global and regional wave modeling activities. *Oceanography* 15, 57–66.
- Komen, G.J., Hasselmann, S., Hasselmann, K., 1984. On the existence of a fully developed wind-sea spectrum. *J. Phys. Oceanogr.* 14, 1271–1285.
- Komen, G.J., Cavaleri, L., Donelan, M., Hasselmann, K., Hasselmann, S., Janssen, P.A.E.M., 1994. *Dynamics and Modelling of Ocean Waves*. Cambridge Univ. Press, 532 pp.
- LeBlond, P.H., Calisal, S.M., Isaacson, M., 1982. *Wave Spectra in Canadian Waters*, Report prepared for the Canadian Department of Fisheries and Oceans by Seasconsult Marine Research Limited, Canadian Contractor Report of Hydrography and Ocean Sciences, No. 6, pp. 193.
- Mansard, E.P.D., Funke, E.R., 1990. On the fitting of JONSWAP spectra to measured sea states. *Int. Conf. Coast. Eng. ASCE*, 464–477.
- Rice, S.O., 1944. The mathematical analysis of random noise. *Bell Sys. Tech. J.* 23, 282–332.
- Rogers, W.E., Wang, D.W., 2007. Directional validation of wave predictions. *J. Atmos. Oceanic Technol.* 24, 504–520.
- Rogers, W.E., Hwang, P.A., Wang, D.W., 2003. Investigation of wave growth and decay in the SWAN model: three regional-scale applications. *J. Phys. Oceanogr.* 33, 366–389.
- Rogers, W.E., Babanin, A.V., Wang, D.W., 2012. Observation-consistent input and whitecapping dissipation in a model for wind-generated surface waves: description and simple calculations. *J. Atmos. Oceanic Technol.* 29, 1329–1346.
- The SWAN team, 2010. *SWAN Scientific and Technical Documentation, SWAN Cycle III version 40.81*, Delft University of Technology, pp. 118. See: <<http://www.swan.tudelft.nl>>.
- Saulnier, J.-P., Clement, A., Falcao, A.F.O., Pontes, T., Prevesto, M., Ricci, P., 2011. Wave groupiness and spectral bandwidth as relevant parameters for the performance assessment of wave energy converters. *Ocean Eng.* 38, 130–147.
- Tolman, H.L., 1991. A Third generation model for wind-waves on slowly varying, unsteady, and inhomogeneous depths and currents. *J. Phys. Oceanogr.* 21 (6), 782–797.
- Tolman, H.L., 2009. *User Manual and System Documentation of WAVEWATCH IIIITM Version 3.14*, Tech. Note, NOAA/NWS/NCEP/MMAB, pp. 220.
- Tolman, H.L., 2011. The impact of nonlinear interaction parameterization on practical wind wave models. In: *Proceedings of 12th International Workshop on Wave Hindcasting and Forecasting*, Hawai'i, USA, pp. 10.
- Tolman, H.L., Balasubramanian, B., Burroughs, L.D., Chalikov, D.V., Chao, Y.Y., Chen, H.S., Gerald, V.M., 2002. Development and implementation of wind-generated ocean surface wave models at NCEP. *Weather Forecasting (NCEP Notes)* 17, 311–333.
- Tsagareli, K.N., 2009. *Numerical investigation of wind input and spectral dissipation in evolution of wind waves*. Ph.D.thesis, University of Adelaide, Australia, pp. 217.
- Tsagareli, K.N., Babanin, A.V., Walker, D.J., Young, I.R., 2010. Numerical investigation of spectral evolution of wind waves. Part 1. Wind input source function. *J. Phys. Oceanogr.* 40, 656–666.
- Van Vledder, G.Ph., 1990. *The directional response of wind waves to turning winds*. Ph.D. thesis Delft University of Technology, pp. 255.
- Van Vledder, G. Ph., 2002. *A subroutine version of the Webb/Resio/Tracy method for the computation of nonlinear quadruplet wave-wave interactions in deep and shallow water*, Alkyon Report 151b, The Netherlands, pp. 155.
- Van Vledder, G.Ph., 2006. *The WRT method for computation of non-linear four-wave interactions in discrete spectral wave models*. *Coastal Eng.* 53, 223–242.
- Van Vledder, G.Ph., Battjes, J.A., 1992. Discussion of “List of sea-state parameters”. *J. Waterway Port Coastal Ocean Eng.* 118 (2), 226–228.
- Van Vledder, G.Ph., Herbers, T.H.C., Jensen, R.E., Resio, D.T., Tracy, B., 2000. *Modelling of non-linear quadruplet wave-wave interactions in operational wave models*. In: *Proceedings of 27th International Conference on Coastal Engineering*, Sydney, Australia, pp. 797–811.
- Van Vledder, G.Ph., Groeneweg, J., van der Westhuysen, A., 2008. *Numerical and physical aspects of wave modelling in a tidal inlet*. In: *Proceedings of 31st International Conference on Coastal Engineering*, Hamburg, Germany, pp. 424–36.
- WAMDI Group, 1988. *The WAM model—A third generation ocean wave prediction model*. *J. Phys. Oceanogr.* 18, 1775–1810.
- The WISE Group (Cavaleri, L., Alves, J.-H.G.M., Arduin, F., Babanin, A.V., Banner, M., Belibassakis, K., Benoit, M., Donelan, M., Groeneweg, J., Herbers, T.H.C., Hwang, P., Janssen, P.A.E.M., Janssen, T., Lavrenov, I.V., Magne, R., Monbaliu, J., Onorato, M., Polnikov, V., Resio, D., Rogers, W.E., Sheremet, A., McKee Smith, J., Tolman, H.L., van Vledder, G., Wolf, J., Young, I.), 2007. *Wave modelling – The state of the art*. *Progr. Oceanogr.* 75, 603–674.
- Young, I.R., 1999. *Wind Generated Ocean Waves*. Elsevier Ocean Engineering Book Series, vol. 2. Elsevier, pp. 288.
- Young, I.R., van Vledder, G.Ph., 1993. The central role of nonlinear wave interactions in wind-wave evolution. *Philos. Trans. R. Soc. London* 342, 505–524.
- Young, I.R., Babanin, A.V., 2006. Spectral distribution of energy dissipation of wind-generated waves due to dominant wave breaking. *J. Phys. Oceanogr.* 36, 376–394.
- Young, I.R., Hasselmann, S., Hasselmann, K., 1987. Computations of the response of a wave spectrum to a sudden change in wind direction. *J. Phys. Oceanogr.* 17, 1317–1338.